Lightning strikes

Scheffer, H.J.

2016

document version
Publisher's PDF, also known as Version of record

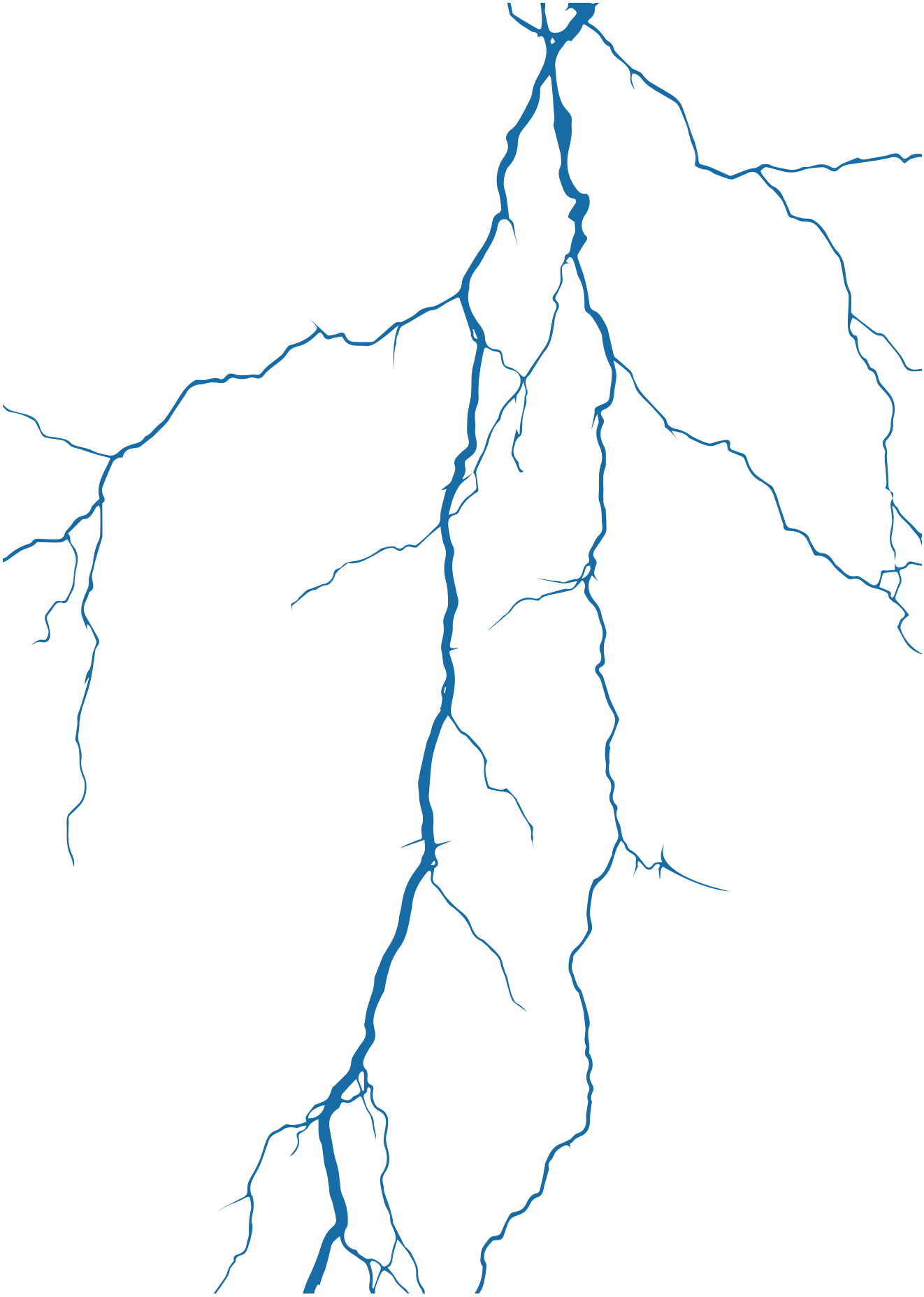

504298-L-bw-Scheffer
Processed on: 21-7-2016

5.2

MR and CT imaging characteristics and ablation zone geometry of locally advanced pancreatic carcinoma treated with irreversible electroporation

Hester J Scheffer*, Laurien GPH Vroomen*, Marleen CAM Melenhorst, Marcus C de Jong, Janneke E van den Bergh, Cornelis van Kuijk, Foke van Delft, Geert Kazemier, Martijn R Meijerink

*Contributed equally

Accepted for publication in European Radiology

504298-L-bw-Scheffer
Processed on: 21-7-2016

Abstract

Purpose

To assess specific imaging characteristics after percutaneous irreversible electroporation (IRE) for locally advanced pancreatic carcinoma (LAPC) with multiphasic contrast-enhanced (ce) MRI and ceCT and to explore the correlation of these characteristics to the development of recurrence.

Methods

Qualitative and quantitative analyses of imaging data were performed on 25 patients treated with percutaneous IRE for LAPC in the prospective PANFIRE-trial. Imaging characteristics of the ablation zone on ceCT and ceMRI were assessed over a 6 month follow-up period. The two-tailed Wilcoxon signed-rank test was performed to compare contrast ratio scores between pre- and post-treatment. To detect early imaging markers for treatment failure, attenuation characteristics at 6 weeks were linked to the area of recurrence within six months.

Results

Post-IRE, diffusion-weighted imaging (DWI) b800 signal intensities decreased in all cases ($p<0.05$). Both ceMRI and ceCT revealed absent or decreased contrast enhancement, with a hyperintense rim on ceMRI. Ablation zone volume increase was noted on both modalities in the first six weeks, followed by a decrease ($p<0.05$). In the patients developing tumor recurrence (5/25), a focal DWI-b800 hyperintense spot at six weeks predated the unequivocal recurrence on CT.

Conclusion

The most remarkable signal alterations after pancreatic IRE were shown by DWI-b800 and ceMRI. These early imaging characteristics may be useful to establish technical success and predict treatment outcome. Whether focal areas of non-altered diffusion restriction truly indicate residual tumor requires longer follow-up and should be the focus of future work.

504298-L-bw-Scheffer
Processed on: 21-7-2016

Introduction

Patients with pancreatic cancer have a poor prognosis. For nonmetastatic disease, the only curative opportunity is surgical resection, unfortunately, only 10%–20% of patients are surgical candidates.[1] Up to 40% of patients present with nonmetastatic but unresectable disease due to vascular encasement (locally advanced pancreatic carcinoma [LAPC] or American Joint Committee on Cancer [AJCC] stage III disease).[1,2] Over the last years, image-guided pancreatic tumor ablation has gained increased interest when surgical options are excluded. Nevertheless, thermal ablation techniques are associated with substantial morbidity and mortality, due to the proximity of large vessels, the pancreatic and common bile duct, and the gastroduodenal wall.[3] Also, the so called 'heat-sink' effect can impede complete ablation.[4]

Recently, irreversible electroporation (IRE) has emerged as a novel ablation technique that potentially circumvents the abovementioned limitations. IRE induces an electric field across cells to alter the cellular transmembrane potential. After reaching a sufficiently high voltage, the phospholipid bilayer structure of the cell membrane is permanently disrupted, inducing apoptosis. It is hypothesized that IRE leaves supporting tissue largely unaffected, preserving the structure of large blood vessels and bile ducts.[5] Since IRE relies on electrical energy, its efficacy is unaffected by the heat-sink effect. This suggests safer and more effective ablation of neoplasms adjacent to large vessels or fragile structures.[6]

Multiple studies have suggested the safety and feasibility of pancreatic IRE,[7–9] but only few have focused on ablation zone imaging characteristics and volumetry post-IRE in the clinical setting.[10–12] Familiarity with post-interventional imaging is essential to determine ablation success and for the detection of recurrence. Since isolated recurrence may be favorable over distant metastasis for patients' prognosis, accurate imaging interpretation following IRE is of considerable importance.[13]

The purpose of the present study was to assess specific imaging characteristics after percutaneous irreversible electroporation (IRE) for locally advanced pancreatic carcinoma (LAPC) with multiphasic contrast-enhanced (ce) MRI and ceCT. Additionally, imaging features prognostic for local recurrence were explored. Secondary aim was to quantify tumor and ablation zone volumes.

Methods

Qualitative and quantitative analyses of imaging data were performed on all patients treated with percutaneous IRE for LAPC in the prospective PANFIRE-trial (Clinicaltrials.gov: NCT01799044). All patients gave written informed consent. The local institutional review board gave approval. Study design and conduct were in accordance with the guidelines for Good Clinical Practice.

Patients and tumors

Twenty-five patients with histologically proven LAPC who met inclusion criteria were included. Prior to study enrollment, all participants were discussed in the multidisciplinary pancreatic tumor board. Inclusion criteria were radiologic confirmation of LAPC stage III (axial diameter ≤5 cm), American Society of Anesthesiologists (ASA) performance status 1-3, and adequate bone marrow, liver and renal function. Exclusion criteria were distant

504298-L-bw-Scheffer
Processed on: 21-7-2016

metastases, history of epilepsy or ventricular arrhythmias, an implanted stimulation device, and a metal biliary stent.

IRE procedure

All procedures were performed under general anesthesia as described previously.[14] A ceCT, using multiplanar image reconstruction, was made to define the three-dimensional tumor measurements. Size and shape, including a 5 mm margin determined the number and configuration of the electrodes (NanoKnife, AngioDynamics, Latham, NY). Three to six electrodes with an exposure length of 15 mm were placed in the outer border or just outside the tumor under CT-guidance. Ablation was performed between all electrode pairs that were separated between 15-24 mm from each other. For larger tumors, the needles were repositioned for one or more overlapping ablations. Per electrode pair a total of 100 pulses of 1500 V/cm and 90 µs were delivered. The AccuSync cardiac synchronization device (Accusync Research Monitor, Milford, Connecticut) was used to synchronize the electric pulses with the patient's electrocardiogram.

Imaging

CeMRI and ceCT scans were performed according to schedule (**table 1**). MRI was performed using a 1.5-Tesla MRI (Signa HDxt, General Electric, Cleveland, Ohio) with an 8-channel phased array coil. Imaging protocol included T2-weighted fast-recovery fast spin echo images (matrix 320×224; field of view [FOV] 400 mm; slice thickness 7 mm), diffusion-weighted images (DWI) (b0, b50 and b800 s/mm2; matrix 160×128; FOV 400 mm; slice thickness 8 mm) and breath-hold unenhanced and contrast-enhanced T1-weighted three-dimensional fat-suppressed spoiled gradient-echo images (matrix 256×256; FOV 350 mm; slice thickness 3 mm; respectively, matrix 256×224; FOV 400 mm; slice thickness 4.4 mm) in the arterial phase (20 s), portal venous phase (60 s), and delayed phase (120 and 180 s) after intravenous injection of gadolinium (Dotarem, Guerbet, Villepinte, France) in a dose of 0.2 mL/kg at 3 mL/s. CT data were acquired using a 64-row MDCT system (Siemens Sensation, Erlangen, Germany). Scanning parameters were 120 kV, 180 mAs and 380 mm FOV. CT was performed after intravenous administration of a 100 mL bolus of nonionic iodinated contrast material (Xenetix 300, Guerbet, Villepinte, France), at 4 mL/s with a scan delay of 40 s for the pancreatic phase and 70 s for the portal venous phase.

Tumor and ablation zone evaluation

Two experienced abdominal radiologists (MCM and JEB) interpreted the ceCT and ceMR images independently. Per sequence, findings were graded systematically according to the specific tumor and ablation zone imaging characteristics compared to the surrounding healthy pancreatic parenchyma, using a region of interest (ROI). MRI intensity was evaluated on an ordinal 7-point scale (---/0/+++). CT density was assessed on an ordinal 3-point scale (-/0/+). Furthermore, the presence and configuration of periablational rim enhancement, intralesional gas pockets and blood residues was evaluated. Discrepancies between the interpreters' findings were solved by consensus.

Table 1. Imaging schedule

Imaging schedule before and after IRE		
0-2 weeks pre-IRE		ceMRI
IRE-procedure	ceCT	
+1 day		ceMRI
+2 weeks		ceMRI
+6 weeks	ceCT	ceMRI
+3, 6, 9, 12 months	ceCT	

Radiologic response was evaluated through Response

Evaluation Criteria in Solid Tumors (RECIST),[15] in which recurrence was defined as a focal or diffuse growing mass within 1 cm of the ablated region compared to the new baseline-scan at 6 weeks post-IRE, accompanied by a substantial cancer antigen (CA) 19.9 rise (duplication compared to baseline). Tumors recurring within six months were considered early recurrences. Histopathologic confirmation was only obtained if patients were eligible for retreatment. To detect possible early imaging markers for treatment failure, a reassessment of the recurrence area was performed.

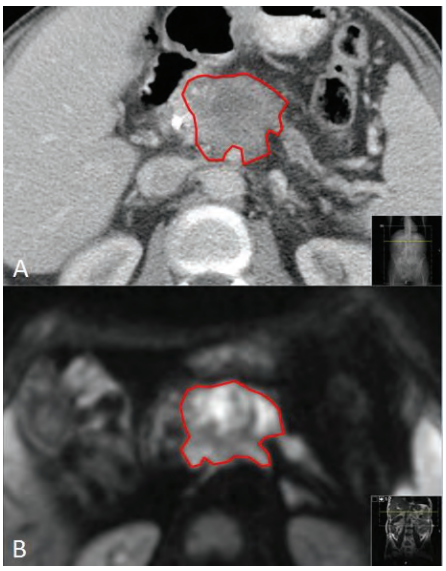

Figure 1: Manually drawn boundary of tumor on (A) ceCT (portal venous phase) and (B) DWI-b800 sequence

Predicted and obtained treatment zone volumes

Tumor and ablation zone volumes were measured by manually drawing the boundary of the tumor and ablation zone on each portal venous ceCT and ceMRI DWI-b800 slice (**figure 1**). The volume of the segmented lesion resulted from the sum of all segmented slice surfaces, multiplied by the reconstruction increment (Caliper method).[16] Patients who developed an early recurrence were excluded from volumetric analysis.

Statistical analyses

Descriptive statistics were used to present results as absolute numbers (normal distribution), median and range (non-normal distribution), or frequencies and percentages (categorical variables). The two-tailed Wilcoxon signed-rank test was performed to compare contrast ratio scores across sequences between pre- and post-treatment. Statistical analyses were performed using SPSS, version 20.0 (SPSS, Chicago, Illinois). The level of statistical significance was set to $p<0.05$. Interobserver-agreement was assessed with κ-statistics.[17] The prognostic accuracy of a focal hyperintense spot on the six-week follow-up DWI-b800 for the development of recurrence within six months post-IRE was determined with sensitivity, specificity, negative predictive value (NPV), and positive predictive value (PPV).

Results

Twenty-five patients with a median age of 61 years (range 41-78) were included for analysis. Tumors were located in the pancreatic head (n=18), body (n=2) and uncinate process (n=5). Needle placement and pulse delivery was successfully performed in all patients. Complications post-IRE were edematous pancreatitis (n=1), duodenal wall ulcer directly adjacent to the ablation zone (n=1), new-onset biliary obstruction (n=3), cholangitis with infected biloma (n=1), and subtotal occlusion of the superior mesenteric artery (n=1).

CeMR imaging

Complete MRI follow-up was accomplished in 21 patients. Four patients were excluded from MR follow-up because of claustrophobia (n=4). CeMRI tumor and ablation zone

findings are shown in table 2. Interobserver agreement was substantial to excellent on DWI-b800, precontrast T1- and postcontrast T1-weighted MRI and moderate to excellent on T2- and postcontrast T1-weighted MRI (table 3).

Prior to IRE, most tumors were markedly hyperintense on T2-weighted images (71%, n=15) and on DWI-b800 (86%, n=18) compared to surrounding normal pancreatic parenchyma. Pancreatic tumors appeared hypointense in 86% (n=18) on both ADC and arterial phase T1-weighted MRI, and in 76% (n=16) on the portal venous phase T1-weighted MRI.

Compared to original tumor intensity, one day post-IRE DWI-b800 MRI signal intensities notably decreased in all cases (p=0.0002), accompanied by a subsequent ADC increase (p=0.0044).

Table 2. Specific tumor and ablation zone imaging characteristics on each MRI sequence (median score)

	Pre-IRE	1 day post-IRE	2 weeks post-IRE	6 weeks post-IRE
T2	+	+	+	+
DWI-b800	++	+	+	+
ADC	-	0	0	0
T1 Precontrast	0	0	0	0
T1 Arterial phase	-	--	--	-
T1 Venous phase	-	---	---	--

+, ++, +++ = hyperintense; 0 = isointense; -, --, --- = hypointense.

Table 3. Interobserver-agreement of ceMRI and ceCT sets (weighted κ-values)

ceMRI	Pre-IRE	1 day post-IRE	2 weeks post-IRE	6 weeks post-IRE
T2	0.768	0.929	0.511	0.910
DWI-b800	0.833	0.918	0.734	1.00
ADC	0.771	0.831	0.412	0.792
T1 precontrast	0.781	1.00	1.00	0.875
T1 arterial phase	0.559	0.750	0.812	0.810
T1 venous phase	1.00	1.00	0.822	0.668

ceCT	Pre-IRE	IRE	6 weeks post-IRE	3 months post-IRE	6 months post-IRE
CT arterial phase	0.802	0.507	0.737	0.545	1.00
CT venous phase	0.505	-		0.704	0.634

Values of κ=0.81–1.00 indicate excellent agreement, κ=0.61–0.80 indicates substantial agreement, κ=0.41–0.60 indicates moderate agreement, κ=0.21–0.40 indicates fair agreement and κ≤0.20 indicates slight agreement (17).

At two and six weeks follow-up, intensity remained low on DWI-b800, in comparison with the initial lesion (p=0,0022 and p=0,0023, respectively) and high on ADC (p=0,0010 and p=0,0022, respectively). One day post-IRE, small areas of diffuse hyperintensity representing blood residues were detected in all ablated areas on precontrast T1-weighted images. At this point, the ablation zone contrast enhancement in the arterial and portal venous phase had decreased in all lesions as compared to initial tumor intensity (p=0,0099 and p=<0,0001). In the portal venous phase, a hyperintense rim surrounding the IRE ablation zone was found in 71% (n=16) both one day and two weeks post-IRE, and was less often identified at six weeks follow-up (29%, n=6). At two and six weeks follow-up, tumor intensity remained low for the arterial phase (p=0,0004 and p=0,033) and portal venous phase (p=0,0001 and p=0,0009). On the T2-weighted sequences, ablation zone intensity during follow-up did not significantly differ from the initial tumor intensity. However, a remarkable hypointense rim surrounding the ablation zone was observed in 52% (n=11) of patients two weeks post-IRE on T2-weighted MRI. An example of typical MRI features is shown in figure 2, corresponding to successfully ablated tumors.

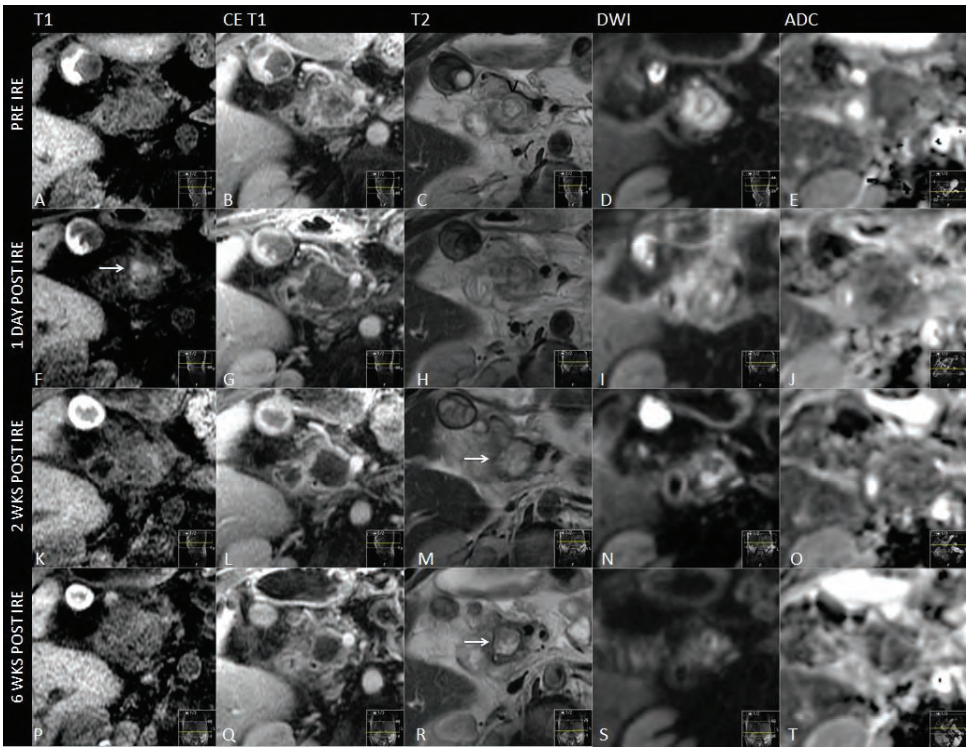

Figure 2: Imaging findings during follow-up on ce-MRI

Prior to IRE: (A) Isointense tumor on T1 sequence (B) Hypointense (-) tumor on T1 sequence (portal venous phase) (C) Hyperintense tumor on T2 sequence (D) Hyperintense (++) tumor on DWI-b800 sequence (E) Hypointense (-) tumor on ADC map.

1 day post-IRE: (F) Isointense IRE ablation zone with small hyperintense blood residues on T1 sequence (G) Hypointense (---) IRE ablation zone plus rim-enhancement surrounding the treated area on T1 sequence (portal venous phase) (H) Hyperintense (+) IRE ablation zone on T2 sequence (I) Hyperintense (+) IRE ablation zone on DWI-b800 sequence (J) Isointense IRE ablation zone on ADC map.

2 weeks post-IRE: (K) Isointense IRE ablation zone on T1 sequence (L) Hypointense (---) IRE ablation zone plus rim-enhancement surrounding the treated area on T1 sequence (portal venous phase) (M) Hyperintense (+) IRE ablation zone plus hypointense rim enhancement surrounding the treated area on T2 sequence (N) Hyperintense (+) IRE ablation zone on DWI-b800 sequence (O) Isointense IRE ablation zone on ADC map.

6 weeks post-IRE: (P) Isointense IRE ablation zone on T1 sequence (Q) Hypointense (--) IRE ablation zone on T1 sequence (portal venous phase) (R) Hyperintense (+) IRE ablation zone plus hypointense rim enhancement surrounding the treated area on T2 sequence (S) Hyperintense (+) IRE ablation zone on DWI-b800 (T) Isointense IRE ablation zone on ADC map.

CeCT imaging

Differences between attenuation pre- and post-IRE in the arterial and portal venous phase were not statistically significant. **Table 4** and **figure 3** show the tumor and ablation zone attenuation characteristics on ceCT. Interobserver agreement was mostly substantial to excellent (**table 3**). Compared to the healthy pancreatic parenchyma the initial tumor appeared either isodense (56%) or hypodense in the arterial phase (44%), and hypodense (72%) in the portal venous phase. Immediately after IRE intralesional and periablational gas pockets were present in all cases. Post-IRE the ablation zones were primarily hypodense in

Table 4. Tumor and ablation zone signal densities on ceCT

	Pre-IRE		Post-IRE	+6 weeks post-IRE		+ 3 months post-IRE		+6 months post-IRE	
	Arterial	Venous	Venous	Arterial	Venous	Arterial	Venous	Arterial	Venous
Hypodense	11 (44%)	18 (72%)	19 (76%)	20 (80%)	23 (92%)	14 (52%)	23 (92%)	9 (56%)	15 (94%)
Isodense	14 (56%)	7 (28%)	6 (24%)	5 (20%)	2 (8%)	11 (48%)	2 (8%)	7 (44%)	1 (6%)
Gas pockets	-	-	25 (100%)	-	-	-	-		

The data shown are number of patients (%). Pre-IRE = before IRE; post-IRE = immediately after IRE.

the arterial phase after 6 weeks and 3- and 6 months (80%, 52%, and 56%, respectively). In the portal venous phase 76% of the ablated areas were slightly hypodense immediately post-IRE; at six weeks and three- and six months follow-up, ablation zones were hypodense in 92%, 92%, and 94%, respectively.

Early recurrence

During a median follow-up period of 6 months (range 3-17), five patients developed an early local recurrence at 2 (n=1), 3 (n=1), 5 (n=2), and 6 (n=1) months, detected on ceCT and accompanied by a substantial CA 19.9 rise. Histopathologic confirmation was obtained in one patient who was subsequently retreated with IRE (figure 4). The four remaining patients were considered unsuitable for retreatment because of excessive disease progression. Targeted analysis of the recurring areas revealed small hyperintense spots adjacent to the overall decreased ablation zone intensity on DWI-b800, which was low on ADC. For this reason all DWI and ADC exams were prospectively re-assessed for the presence of these marginal spots by both reviewers (MCM and JEB). Interobserver agreement was substantial (κ=0.674). In 4/5 patients a marginal spot showing diffusion restriction correlated to early recurrence. In a fifth patient patchy hyperintensity at 6 weeks evolved into extensive local recurrence after 6 months. However, a marginal spot was also identified in 3/16

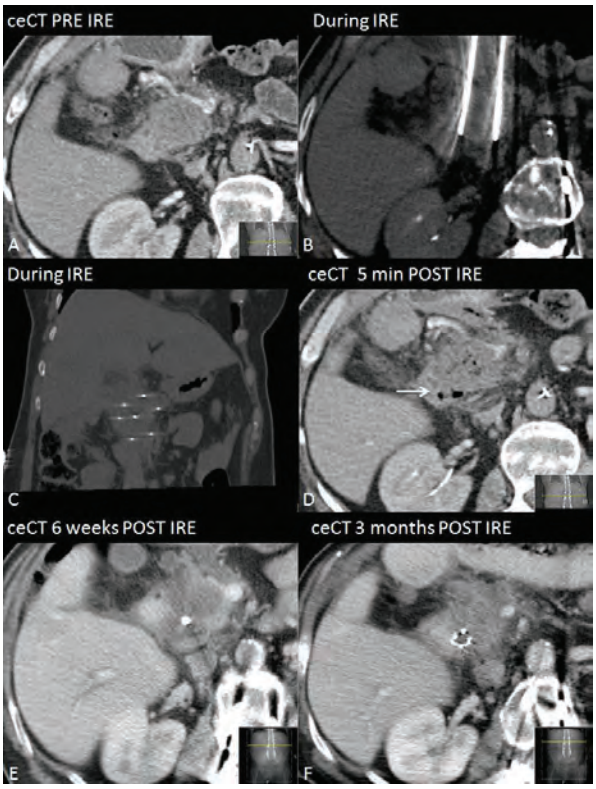

Figure 3: . Imaging findings during follow-up on ceCT. (A) Isoattenuating tumor on ceCT pre-IRE (B) CT-guided placement of electrodes around the outer border of the tumor (C) Confirmation of correct electrode configuration according to the treatment plan with a nonenhanced CT scan (D) Hypoattenuating IRE ablation zone with intralesional gas pockets immediately after IRE (E) Hypoattenuating IRE ablation zone at six weeks follow-up (F) Hypoattenuating IRE ablation zone at three months follow-up.

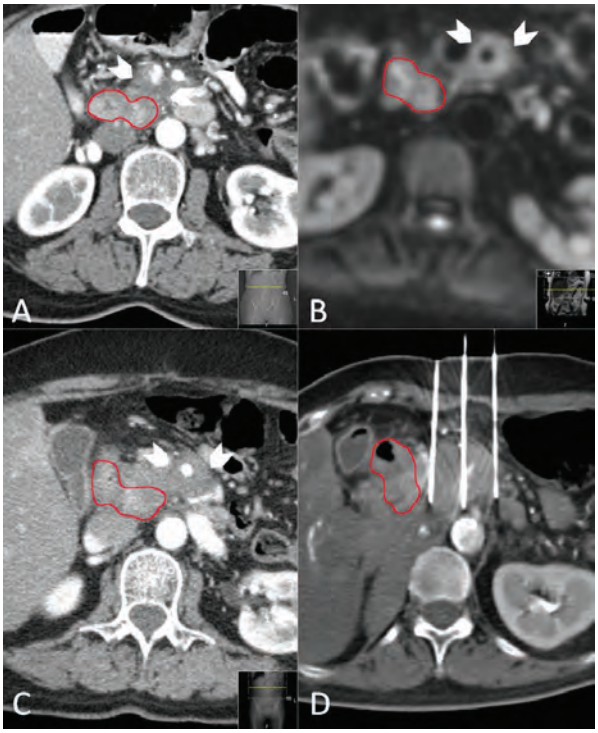

Figure 4: The development of a local recurrence. Red line = duodenum. (A) CeCT pre-IRE showing the initial tumor (white arrowheads) that was treated with IRE (B) MR DWI-b800 6 weeks post-IRE showing new hyperintensity around the superior mesenteric artery (white arrowheads) (C) CeCT 4 months post-IRE showing evident local recurrence (white arrowhead) (D) re-IRE of the local recurrence.

patients without early relapse (sensitivity 100%, specificity 81%, NPV 100%, and PPV 63%).

Tumor and ablation zone volumes

Ablation zones on both ceCT and DWI-b800 were difficult to delineate from the surrounding pancreatic parenchyma due to intralesional gas pockets, blood residues and surrounding tissue edema.

CeMR imaging

The volume of one ablation zone prior to treatment and six weeks post-IRE could not be defined. Median tumor volume 0-2 weeks prior to intervention was 19 mL (range 6-58). One day post-IRE median ablation zone volume was 49 mL (range 16-100). At two weeks follow-up, median volume was reduced to 16 mL (range 7-98). The median ablation zone volume remained mostly stable at six weeks follow-up (14 mL, range 5-71) (**figure 5**).

CeCT imaging

Volumes prior to IRE (n=2), immediately post-IRE (n=8), six weeks post-IRE (n=4), three months post-IRE (n=1) and six months (n=1) could not be precisely determined due to poorly demarcated margins of the ablation zone. A median tumor volume of 15 mL (range 4-98) was measured on ceCT pre-IRE. Median ablation zone volume directly after the intervention was 31 mL (range 19-150). On follow-up examinations after six weeks, median volume had decreased to 17 mL (range 2-59). Eventually, ablation zone volume was equal to original tumor volume at three months follow-up (median 22 mL, range 4-78) and six months (median 28 ml, range 8-64)(**figure 5**).

Discussion

Evaluation of tumor response after ablation is important to define treatment success and to guide future therapy.[18] Knowledge of postinterventional MR and CT findings is essential for accurate interpretation of the ablated area. Familiarity with these characteristics prevents

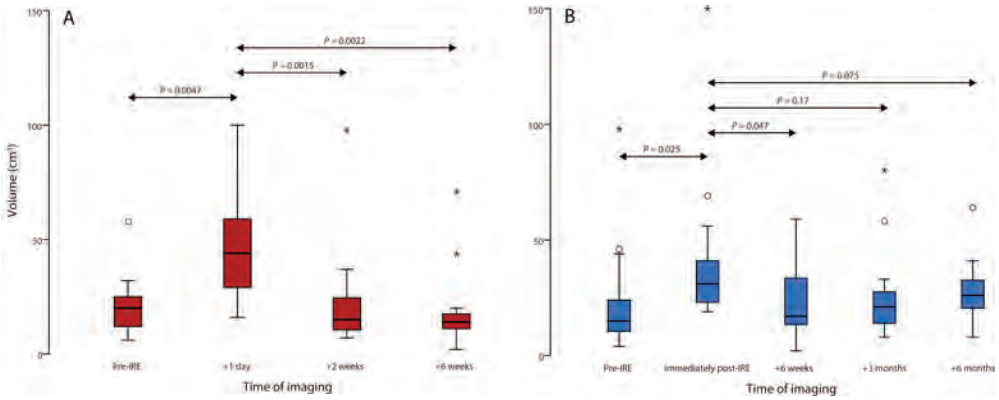

Figure 6: Box plots of tumor and ablation zone volumes pre- and post-IRE of (A) MRI and (B) CT; p-values from Wilcoxon signed-rank test.

confusion between normal or less typical postablational changes and residual or recurrent disease. In addition, timely recognition of IRE-related complications and vital tumor allows for expedited management and possible retreatment. In this study, the evolution of ablation zones based on ceMRI and ceCT was reviewed over a follow-up period of 90 days.

In the liver, compared to the surrounding normal parenchyma, a well-demarcated ablation zone is commonly visible on CT and MRI post-IRE.[11,19] Also, IRE ablation zones in the liver depict a transient peripheral hyperenhancing rim.[11,19] Since generally little healthy pancreatic tissue surrounds the pancreatic tumor, in our study the ablation zone was often ill-defined on MRI and especially on CT. Also, the presence of more edema within the ablation zone often impeded precise ablation zone delineation.

Literature on post-IRE MRI is scarce and predominantly involves the liver; imaging data of pancreatic IRE in humans is not available yet. A reasonable explanation for the observed hyperintense rim surrounding the ablation zone post-IRE is reactive hyperemia of edematous inflammatory origin.[20,21] However, it cannot be excluded that this rim still contains residual disease and longer follow-up is needed to explore the exact significance. The remarkable hypointense rim that we found on T2 at two weeks suggests hemosiderin deposition[22] resulting from degradation of the extravasated erythrocytes in the periphery of the ablation zone.[23]

Post-IRE, arterial and portal venous phase CT attenuation decreased in nearly all patients. This decline in enhancement is in line with the observed postcontrast MRI findings which may be indicative for accurate tumor therapy response.[24] The observed intralesional gas pockets may be caused by electrolysis of water into hydrogen and oxygen caused by the electric pulses,[23] or by vaporization due to heat development, or by a combination of these mechanisms.

Initial post-IRE examinations revealed a notable volume increase on ceCT and ceMRI, followed by a decrease during follow-up. The calculated volumes varied widely between the two modalities, which is caused by the difficult ablation zone delineation from surrounding structures. Studies investigating the size and shape of the IRE ablation zone have predominantly correlated imaging findings to histology in animal studies. Overall,

the radiological ablation zone size as measured on CT and MRI-DWI correlates well with the histologic ablation zone.[20,25,26] In addition, studies suggested that ablation zone size and shape depend on the IRE parameters used and on the type of tissue ablated.[27] There is clear concordance between our findings and preclinical and early clinical studies that describe a reduction of the size of the ablated area over several weeks,[6,11,12,20] resulting from the clearance of cellular debris aided by the preservation of larger vessels.[6,20]

The World Health Organization (WHO) criteria and RECIST criteria, depend on decrease in tumor size.[28,29] However, decrease in viable cell mass is not always reflected by changes in tumor size.[30] Exclusive reliance on tumor size does therefore not provide a complete assessment of tumor response and may lead to inaccurate conclusions.[29] A preferable method of post-IRE treatment evaluation is to combine tumor and ablation zone sizes with functional information such as alterations in enhancement and diffusion.[31]

CT is the standard imaging modality used for follow-up of pancreatic cancer and has an accuracy of 93.5% for detecting locally recurrent tumor after pancreaticoduodenectomy using RECIST.[32] Since all five patients showed DWI-b800 hyperintensity and low ADC values at the site of eventual recurrence at six weeks, DWI-b800 and ADC may be useful to predict early recurrence or incomplete ablation, similar to imaging after hepatic ablation.[33] This may allow for earlier retreatment. However, the presumed hemosiderin deposition mentioned above may limit the capability of DWI-b800 to interpret the ablated area, in particular when the treatment zone is small, as susceptibility artifacts may obscure small areas of recurrence or create false-positives. Clearly, larger numbers are needed to validate this finding.

^{18}F-fluorodeoxyglucose positron emission tomography (^{18}F-FDG PET) CT has demonstrated better diagnostic accuracy compared with ceCT [34] and even MRI (without DWI-b800)[35] in the diagnosis of pancreatic cancer. Also, ^{18}F-FDG PET is increasingly used to assess tissue response to chemoradiation for LAPC. A recent study showed the difference in maximum standardized uptake value (SUVmax) pre- and post-chemoradiation for LAPC was an independent predictor of clinical outcome.[34] In this study, ^{18}F-FDG PET was not performed, but the value of ^{18}F-FDG PET as a predictor for ablation success after pancreatic IRE should be investigated in future studies.

The greatest limitation of this study was the sample size, which precluded a meaningful quantitative data-analysis with respect to recurrences, therefore, no multivariable analyses were considered. Furthermore, histopathologic confirmation of recurrence was obtained in only one patient. Given the lack of clinical consequences and the associated risk of biopsy, no histopathologic confirmation was obtained in the remaining four patients. Another drawback was the often poorly delineated ablation zone caused by a peri-ablational inflammatory response, which renders the accuracy of the calculated volumes uncertain, especially on CT.

In conclusion, the most remarkable signal alterations after pancreatic IRE are shown by DWI-b800 and postcontrast T1-weighted MRI and these imaging characteristics may be useful to predict complete ablation and early recurrence. Future studies should elaborate whether imaging characteristics post-IRE can predict treatment outcome and stratify patients for potential retreatment.

References

1. Bilimoria KY, Bentrem DJ, Ko CY, et al. Validation of the 6th edition AJCC Pancreatic Cancer Staging System: report from the National Cancer Database. Cancer. 2007;110:738–744.
2. Callery MP, Chang KJ, Fishman EK, Talamonti MS, William Traverso L, Linehan DC. Pretreatment assessment of resectable and borderline resectable pancreatic cancer: expert consensus statement. Ann Surg Oncol. 2009;16:1727–1733.
3. Pandya GJ, Shelat VG. Radiofrequency ablation of pancreatic ductal adenocarcinoma: The past, the present and the future. World J Gastrointest Oncol. 2015;7:6–11.
4. Pezzilli R, Serra C, Ricci C, et al. Radiofrequency ablation for advanced ductal pancreatic carcinoma: is this approach beneficial for our patients? A systematic review. Pancreas. 2011;40:163–165http://www.ncbi.nlm.nih.gov/pubmed/21160378. Accessed August 13, 2014.
5. Lee EW, Thai S, Kee ST. Irreversible electroporation: a novel image-guided cancer therapy. Gut Liver. 2010;4 Suppl 1:S99–S104.
6. Rubinsky B, Onik G, Mikus P. Irreversible electroporation: a new ablation modality--clinical implications. Technol Cancer Res Treat. 2007;6:37–48.
7. Martin RCG, Kwon D, Chalikonda S, et al. Treatment of 200 Locally Advanced (Stage III) Pancreatic Adenocarcinoma Patients With Irreversible Electroporation: Safety and Efficacy. Ann Surg. 2015;262:486–494.
8. Paiella S, Butturini G, Frigerio I, et al. Safety and Feasibility of Irreversible Electroporation (IRE) in Patients with Locally Advanced Pancreatic Cancer: Results of a Prospective Study. Dig Surg. 2015;32:90–97.
9. Scheffer HJ, Nielsen K, de Jong MC, et al. Irreversible electroporation for nonthermal tumor ablation in the clinical setting: a systematic review of safety and efficacy. J Vasc Interv Radiol. 2014;25:997–1011.
10. Neal RE, Garcia PA, Robertson JL, Davalos R V. Experimental characterization and numerical modeling of tissue electrical conductivity during pulsed electric fields for irreversible electroporation treatment planning. IEEE Trans Biomed Eng. 2012;59:1076–1085.
11. Dollinger M, Jung E-M, Beyer L, et al. Irreversible Electroporation Ablation of Malignant Hepatic Tumors: Subacute and Follow-up CT Appearance of Ablation Zones. J Vasc Interv Radiol. 2014;25:1589–1594.
12. Akinwande O, Ahmad SS, Van Meter T, Schulz B, Martin RCG. CT Findings of Patients Treated with Irreversible Electroporation for Locally Advanced Pancreatic Cancer. J Oncol. Hindawi Publishing Corporation; 2015;2015:680319.
13. Hidalgo M. Pancreatic Cancer. N Engl J Med. 2010;362:1605–1617.
14. Nielsen K, Scheffer HJ, Vieveen JM, et al. Anaesthetic management during open and percutaneous irreversible electroporation. Br J Anaesth. 2014;113:985–992.
15. Eisenhauer EA, Therasse P, Bogaerts J, et al. New response evaluation criteria in solid tumours: revised RECIST guideline (version 1.1). Eur J Cancer. 2009;45:228–247.
16. Monsky WL, Raptopoulos V, Keogan MT, et al. Reproducibility of linear tumor measurements using PACS: comparison of caliper method with edge-tracing method. Eur Radiol. 2004;14:519–525.
17. Viera AJ, Garrett JM. Understanding interobserver agreement: the kappa statistic. Fam Med. 2005;37:360–363.
18. Vossen JA, Buijs M, Kamel IR. Assessment of tumor response on MR imaging after locoregional therapy. Tech Vasc Interv Radiol. 2006;9:125–132.
19. Neal II RE, Cheung W, Kavnoudias H, Thomson KR. Spectrum of imaging and characteristics for liver tumors treated with irreversible electroporation. J Biomed Sci Engin. 2012;2012:11–15.
20. Appelbaum L, Ben-David E, Sosna J, Nissenbaum Y, Goldberg SN. US findings after irreversible electroporation ablation: radiologic-pathologic correlation. Radiology. Radiological Society of North America, Inc.; 2012;262:117–125.

21. Lee EW, Chen C, Prieto VE, Dry SM, Loh CT, Kee ST. Advanced hepatic ablation technique for creating complete cell death: irreversible electroporation. Radiology. 2010;255:426–433.
22. Chavhan GB, Babyn PS, Thomas B, Shroff MM, Haacke EM. Principles, techniques, and applications of T2*-based MR imaging and its special applications. Radiographics. 29:1433–1449.
23. Scheffer HJ, Nielsen K, van Tilborg a a JM, et al. Ablation of colorectal liver metastases by irreversible electroporation: results of the COLDFIRE-I ablate-and-resect study. Eur Radiol. 2014;24:2467–2475.
24. Lencioni R, Llovet JM. Modified RECIST (mRECIST) assessment for hepatocellular carcinoma. Semin Liver Dis. 2010;30:52–60.
25. Guo Y, Zhang Y, Nijm GM, et al. Irreversible electroporation in the liver: contrast-enhanced inversion-recovery MR imaging approaches to differentiate reversibly electroporated penumbra from irreversibly electroporated ablation zones. Radiology. 2011;258:461–468.
26. Legrand L, Duchatelle V, Molinié V, Boulay-Coletta I, Sibileau E, Zins M. Pancreatic adenocarcinoma: MRI conspicuity and pathologic correlations. Abdom Imaging. 2014.
27. Ben-David E, Ahmed M, Faroja M, et al. Irreversible electroporation: treatment effect is susceptible to local environment and tissue properties. Radiology. Radiological Society of North America; 2013;269:738–747.
28. Miller AB, Hoogstraten B, Staquet M, Winkler A. Reporting results of cancer treatment. Cancer. 1981;47:207–214.
29. Therasse P, Arbuck SG, Eisenhauer EA, et al. New guidelines to evaluate the response to treatment in solid tumors. European Organization for Research and Treatment of Cancer, National Cancer Institute of the United States, National Cancer Institute of Canada. J Natl Cancer Inst. 2000;92:205–216.
30. Ahmed M, Solbiati L, Brace CL, et al. Image-guided Tumor Ablation: Standardization of Terminology and Reporting Criteria-A 10-Year Update. Radiology. 2014;273:241–260.
31. Goldberg SN, Grassi CJ, Cardella JF, et al. Image-guided tumor ablation: standardization of terminology and reporting criteria. J Vasc Interv Radiol. 2009;20:S377–S390.
32. Mortelé KJ, Lemmerling M, Hemptinne B de, Vos M De, Bock G De, Kunnen M. Original article Postoperative findings following the Whipple procedure : determination of prevalence and morphologic abdominal CT features. Eur Radiol. 2000;10:123–128.
33. Sainani NI, Gervais D a, Mueller PR, Arellano RS. Imaging after percutaneous radiofrequency ablation of hepatic tumors: Part 2, Abnormal findings. AJR Am J Roentgenol. 2013;200:194–204.
34. Topkan E, Parlak C, Kotek A, Yapar AF, Pehlivan B. Predictive value of metabolic 18FDG-PET response on outcomes in patients with locally advanced pancreatic carcinoma treated with definitive concurrent chemoradiotherapy. BMC Gastroenterol. 2011;11:123.
35. Kauhanen SP, Komar G, Seppänen MP, et al. A prospective diagnostic accuracy study of 18F-fluorodeoxyglucose positron emission tomography/computed tomography, multidetector row computed tomography, and magnetic resonance imaging in primary diagnosis and staging of pancreatic cancer. Ann Surg. 2009;250:957–963.